

## Strain Relief in Cu-Pd Heteroepitaxy

Yafeng Lu,<sup>1,2</sup> M. Przybylski,<sup>1</sup> O. Trushin,<sup>3</sup> W. H. Wang,<sup>1</sup> J. Barthel,<sup>1</sup> E. Granato,<sup>4</sup> S. C. Ying,<sup>5</sup> and T. Ala-Nissila<sup>5,6</sup>

<sup>1</sup>Max-Planck-Institut für Mikrostrukturphysik, Weinberg 2, D-06120 Halle, Germany

<sup>2</sup>Northwest Institute for Nonferrous Metal Research, P.O. Box 51, Xian, Shaanxi 710016, People's Republic of China

<sup>3</sup>Institute of Microelectronics and Informatics of Russian Academy of Sciences, Universitetskaya 21, Yaroslavl 150007, Russia

<sup>4</sup>Laboratório Associado de Sensores e Materiais, Instituto Nacional de Pesquisas Espaciais, 12245-970 São José dos Campos, SP Brasil

<sup>5</sup>Department of Physics, Brown University, Providence, Rhode Island 02912, USA

<sup>6</sup>Laboratory of Physics, Helsinki University of Technology, FIN-02015 HUT, Espoo, Finland

(Received 11 November 2004; published 13 April 2005)

We present experimental and theoretical studies of Pd/Cu(100) and Cu/Pd(100) heterostructures in order to explore their structure and misfit strain relaxation. Ultrathin Pd and Cu films are grown by pulsed laser deposition at room temperature. For Pd/Cu, compressive strain is released by networks of misfit dislocations running in the [100] and [010] directions, which appear after a few monolayers (ML) already. In striking contrast, for Cu/Pd the tensile overlayer remains coherent up to about 9 ML, after which multilayer growth occurs. The strong asymmetry between tensile and compressive cases is in contradiction with continuum elasticity theory and is also evident in the structural parameters of the strained films. Molecular dynamics calculations based on classical many-body potentials confirm the pronounced tensile-compressive asymmetry and are in good agreement with the experimental data.

DOI: 10.1103/PhysRevLett.94.146105

PACS numbers: 68.55.-a, 68.35.Gy, 81.15.Fg

Heteroepitaxy with different thicknesses ranging from monoatomic layers up to micrometers produces various structures and is one of the most important routes to artificially obtain functional materials and devices. Stress and its relaxation due to an interface lattice mismatch are an essential problem in the heterostructures. Classical continuum theory defines the concept of an equilibrium critical thickness  $h_c$ , above which the lattice stress relaxes with the introduction of a misfit dislocation (MD) [1]. The critical thickness is determined by energy balance between strain energy buildup and strain relief due to dislocation nucleation in the mismatched structure. The value of  $h_c$  predicted by the continuum theory, however, often does not agree with experiments. Moreover, the critical thickness in the continuum elasticity theory is independent of the strain type, be it tensile or compressive. Atomic details of the interface structure, such as surface steps and surface roughness, are usually ignored. Actual stress relaxation of coherent strained films is kinetically limited, typically with high barriers. Recently, atomistic studies on model systems have been done to determine the transition paths and energy barriers from coherent to incoherent states in real epitaxial films [2–4]. One of the main findings has been a striking asymmetry between the tensile and compressive cases, due to the anharmonicity and asymmetry of the atomic interactions [3,4]. Further, the concept of a size-dependent mesoscopic mismatch has been proposed to explain strain relaxations in the early stage of homoepitaxial and heteroepitaxial metal growth on the atomic scales [5].

In this Letter, we present results from a combined experimental and theoretical study on a model system of Cu-Pd heteroepitaxy grown by pulsed laser deposition (PLD).

The bulk lattice parameters of Cu and Pd are  $a_{\text{Cu}} = 3.61 \text{ \AA}$  and  $a_{\text{Pd}} = 3.89 \text{ \AA}$ , respectively. The lattice misfit induces a large compressive ( $m = -7.2\%$ ) strain in the Pd overlayer on Cu(100) and a tensile ( $m = 7.8\%$ ) strain for the Cu overlayer on Pd(100). The Pd films on Cu(100) and the Cu films on Pd(100) were grown by PLD in a multichamber UHV system with a base pressure  $p < 5 \times 10^{-11}$  mbar, and  $p < 2 \times 10^{-10}$  mbar during deposition. Prior to deposition the copper and palladium substrates were cleaned by cycles of Ar<sup>+</sup> sputtering followed by annealing at 873 K for the Cu substrate or 950 K for the Pd substrate until clean Auger electron spectroscopy spectra, sharp low-energy electron diffraction (LEED) spots, and atomically smooth terraces under scanning tunneling microscopy (STM) were observed. The substrate temperature was kept at room temperature during deposition. The substrate was placed about 100–130 mm away from the targets. A KrF excimer laser beam (wavelength 248 nm, pulse duration 34 ns, typical pulse energy 300–350 mJ, and pulse repetition rate 3–5 Hz) was focused onto the targets. During deposition the growth process was monitored by a reflection high energy electron diffraction (RHEED). All STM measurements were performed in the constant current mode at a 0.2–0.5 V positive tip bias and a 0.1–0.5 nA tunneling current. Compared to thermal deposition, an extremely high instantaneous flux of atoms in PLD favors much larger nucleation density [6,7]. This helps to suppress the formation of a Cu(001)<sub>c</sub>(2 × 2)-Pd ordered alloy in the initial growth stage for Pd/Cu(100) [8] and the phase transition at 1 ML from fcc to body-centered tetragonal structure for Cu/Pd(100) [9]. Even though the present STM setup does not provide a direct distinction of the Pd and Cu atoms, neither pits in the substrate surface nor

eroded substrate step edges show any evidence of Cu-Pd interlayer mixing. Moreover, the surface area covered by the islands for submonolayer coverages, as determined from STM images, is always consistent with the coverage from RHEED. The RHEED data confirm the layer-by-layer growth mode for both systems. It persists up to at least 5–6 ML in Cu-Pd heteroepitaxy.

Figures 1(a)–1(d) display STM images taken at room temperature for Pd films on Cu(100). For submonolayer Pd at 0.5 ML, many islands with a monolayer height of about 1.80 Å were observed as shown in the inset of Fig. 1(a). With increasing Pd thickness such islands are always formed on a completely filled underlayer up to a total thickness of about 3–4 ML, indicating an ideal 2D growth mode. Above 4 ML a striking feature is the appearance of misfit dislocations as marked by many protruding stripes with an average height of  $\Delta h = (0.57 \pm 0.10)$  Å [see Figs. 1(c) and 1(d)], by which the compressive stress in the Pd film relaxes efficiently. They align nearly regularly along the [100] and [010] directions. The average spacing of MD lines is  $(7.09 \pm 0.30)$  nm for 4.8 ML. The layer-by-layer growth persists up to 6 ML, after which the multilayer growth mode occurs.

The corresponding layer-by-layer growth mode for PLD Cu films on Pd(100) has also been confirmed by STM images as indicated in Fig. 2. At 0.85 ML, second layer nucleation is not found, while in the 2.1 ML thick film more than 95% of the second layer is accomplished [Figs. 2(b) and 2(c)]. At 2.1 ML, few of the islands in the third layer have a preferential orientation, whereas at

3.05 ML most of the fourth layer islands are rectangular along the  $\langle 110 \rangle$  directions. With increasing Cu thickness to 6.0 ML, 90% of the sixth layer is completed, where nearly all the pits in the sixth layer and the seventh layer islands are rectangular. Above 6 ML the morphology of Cu films is changed because of the multilayer growth mechanism. A typical image for 9.0 ML is given in Fig. 2(f). Four layers appear simultaneously on the surface. Moreover, only 70% of the ninth layer is completed while the remaining 30% appears as the 10th and 11th layers. It should be pointed out that the height or depth of all (ir)regular islands and pits is about 1.65 Å until 9.0 ML as shown in the inset of Fig. 2(e). This vertical magnitude corresponds to the interlayer spacing of highly strained fcc Cu [10]. In PLD Cu films on Pd(100) we have not found any trace of dislocation nucleation up to 9 ML. Above 9 ML, the multilayer island structure with the  $\langle 110 \rangle$  orientation is still visible and the film surface becomes more and more rough.

IV-LEED measurements of the specularly scattered electron beam were done to obtain structural information on the films. The average interlayer spacing of PLD films was calculated from LEED intensity of the (00) diffraction beam vs energy curves based on a kinetic model [11]. Figure 3 gives the layer thickness dependence of the interlayer distance for both systems. In the case of Pd/Cu(100) films, the interlayer distance is about 1.82(5) Å up to 3 ML, very close to the value of the Cu substrate, and increases rapidly above 3 ML to reach the value of bulk Pd. For Cu on Pd(100) up to 10 ML, the value stays constant ( $\approx 1.64$  Å). This agrees well with the measured height of monolayer islands by STM. Above 10 ML the interlayer spacing gradually increases close to the value of bulk fcc Cu at a coverage of 20 ML.

The actual in-plane lattice constant of deposited films was obtained *in situ* by measuring the spacing between the

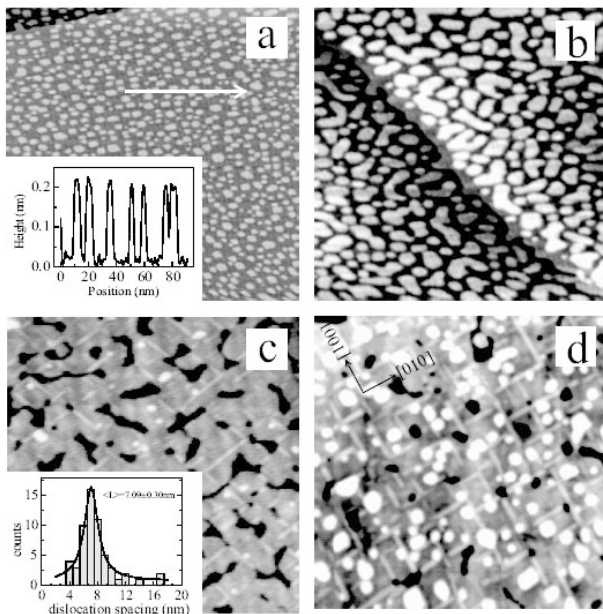


FIG. 1. STM images for (a) 0.5 ML Pd ( $200 \times 200$  nm<sup>2</sup>), (b) 1.6 ML Pd ( $200 \times 200$  nm<sup>2</sup>), (c) 4.8 ML Pd ( $100 \times 100$  nm<sup>2</sup>), and (d) 6.0 ML Pd ( $100 \times 100$  nm<sup>2</sup>) deposited at 300 K.

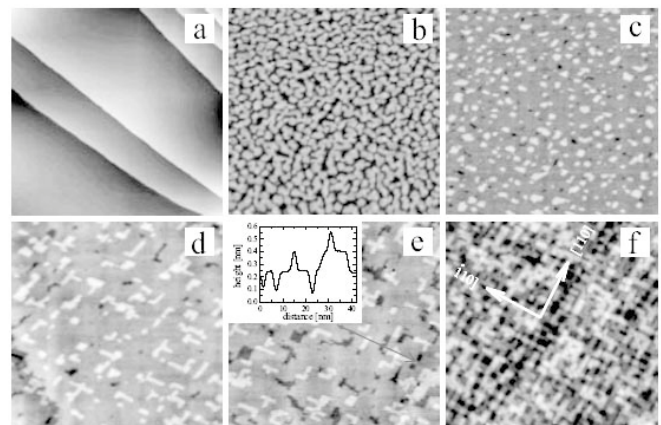


FIG. 2. STM images for (a) clean Pd(100) substrate ( $500 \times 500$  nm<sup>2</sup>), (b) 0.85 ML Cu ( $100 \times 100$  nm<sup>2</sup>), (c) 2.1 ML Cu ( $100 \times 100$  nm<sup>2</sup>), (d) 3.05 ML Cu ( $100 \times 100$  nm<sup>2</sup>), (e) 6.0 ML Cu ( $100 \times 100$  nm<sup>2</sup>), and (f) 9.0 ML Cu ( $100 \times 100$  nm<sup>2</sup>) deposited at 300 K.

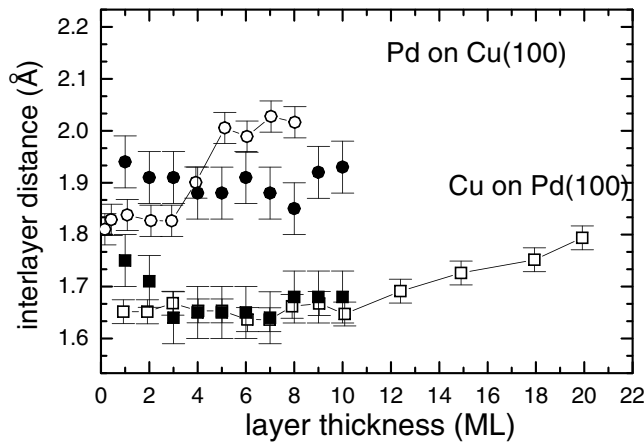


FIG. 3. Perpendicular interlayer distance calculated based on a kinetic model from LEED intensity of the (00) diffraction beam vs energy curves. The change of the interlayer distance occurs at about 3–4 ML for Pd/Cu(100) films and at about 10 ML for Cu/Pd(100) films. Assuming a pseudomorphic growth up to 3 ML for Pd on Cu(100) and 10 ML for Cu on Pd(100), PLD films can be identified as fcc Pd and face-centered tetragonal (fct) Cu structures. The results from experimental and theoretical work at 300 K are indicated by open and solid symbols, respectively. The lines are guides to the eye.

reciprocal lattice rods in the RHEED image. The RHEED spacing of substrates serves as a reference. The in-plane lattice strain is defined as  $(a_{\text{bulk}} - a_{\text{film}})/a_{\text{bulk}}(\%)$ . Figure 4 gives the measured data. For Pd/Cu(100), the measured in-plane strain exhibits a gradual decrease with increasing thickness of the Pd film. The compressive strain is nearly fully relaxed at 9 ML. In contrast, the in-plane tensile strain shows a very different thickness dependence in the case of PLD Cu films on Pd(100). Until 9 ML only a 0.6% reduction in the tensile strain is found. Above 9 ML a steplike decrease is visible and a residual strain is observed until 20 ML.

The most striking discovery in our data is the strong asymmetry in the strain relaxation behavior between the tensile and compressive strained films. This result is in direct disagreement with the continuum elasticity theory, which predicts a symmetrical behavior for tensile and compressive systems.

In any growth mode, there is always the question whether the final configuration is dictated by kinetic considerations or whether it corresponds to a true thermodynamic equilibrium state. Given the lack of precise characterization of the PLD growth conditions, a full theoretical modeling of the kinetic growth process under the experimental conditions is unfeasible. Instead, we have chosen to perform equilibrium molecular dynamics simulations of the epitaxial layer after deposition. The object here is to study the thermal excitation and nature of dislocations in the epitaxial film and to see whether they can account for the observed stress relaxation and tensile-

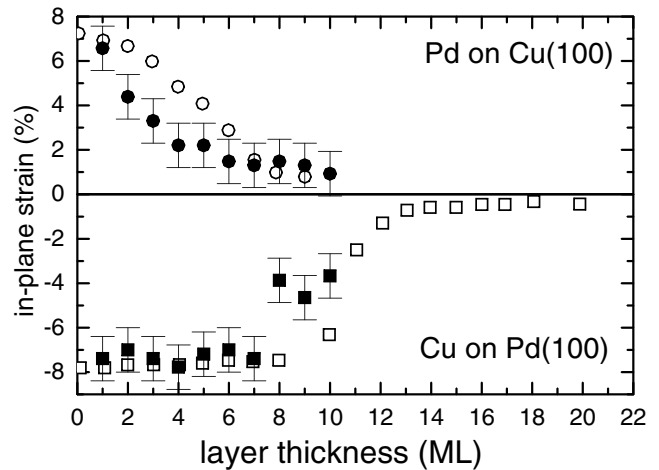


FIG. 4. In-plane lattice strain derived from the separation of the first order rods in the RHEED pattern as a function of Pd or Cu coverages. Our results from experimental and theoretical work at 300 K are indicated by open and solid symbols, respectively. See the text for details.

compressive asymmetry in Cu-Pd heterostructures. Our atomistic model contains five layers of substrates and a varying number of film layers. The two bottom layers of the substrate were fixed. Periodic boundary conditions were applied in the plane parallel to the surface. The lateral size of the systems studied varied between  $20 \times 20$  to  $40 \times 40$ . Interatomic forces between particles in the system were computed using embedded atom model (EAM) potentials for Cu and Pd [12]. The initial configuration of the film has adatoms occupying fcc positions in registry with the substrate.

For Pd/Cu(100), after thermal equilibrium is reached at 300 K, the system relaxes and gains partial strain relief through generation of misfit dislocations starting at 2 ML and above. To facilitate a direct comparison with the experimental data in Fig. 3, we computed from our simulations the average interlayer distance for the top layers of the film (up to three to take into account the surface sensitivity of LEED). We also computed the average in-plane lattice constant for the top three surface layers and then evaluated the in-plane strain using the bulk value of the adsorbate as a reference. The dependence of these values on the film thickness is shown in Fig. 4. There is a good qualitative agreement between the theoretical results with the experimental observation showing continuous relief of in-plane strain through the misfit dislocations. The exact nature of the misfit dislocations is rather complicated, varying both as a function of film thickness and lateral size. In Fig. 5, we show a typical configuration for a film of 7 ML thickness and lateral size  $20 \times 20$  obtained by molecular dynamics annealing through heating to 500 K, followed by cooling to 0 K. This shows a Pd film with misfit dislocations visibly aligned along the  $\langle 100 \rangle$  direction

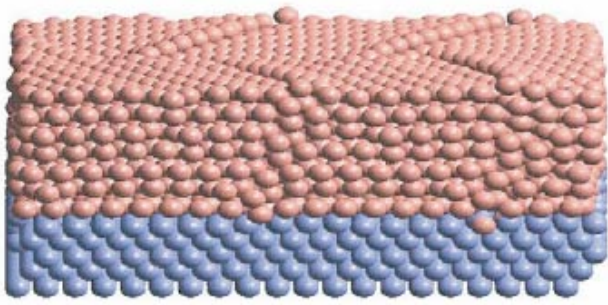


FIG. 5 (color online). Typical configuration of stacking faults for 7 ML Pd on Cu(100) based on molecular dynamics annealing. The lateral size is  $20 \times 20$  atom<sup>2</sup>. The misfit dislocations orientate along the  $\langle 100 \rangle$  direction of the substrate.

of the substrate, in agreement with the experimental observations.

Simulation studies were also performed for Cu/Pd(100). Here, in agreement with the experimental observation, the theory shows a striking difference from the Pd/Cu(100) system. The pseudomorphic strained fct structure for the Cu film remains stable up to about 9 ML. Then strain is gradually released through localized surface defects such as vacancies and adatoms, rather than the misfit dislocation mechanism observed in Pd/Cu(100). The theoretical results for the average interlayer distance of the film and the in-plane strain for the top surface layers as a function of the film thickness are shown in Figs. 3 and 4, respectively. The theory again is in good agreement with the experimental data, indicating a stable highly strained epitaxial state below 9 ML.

In conclusion, we have studied the stress relaxation mechanism in Cu-Pd heteroepitaxy both through PLD experiments and numerical simulations. The experimental data show that for Pd/Cu(100), the in-plane stress is relaxed almost immediately above 1 ML, whereas Cu/Pd(100) remains coherent up to about 9 ML. While these observations contradict predictions from the continuum theory, they are confirmed by our atomistic simulations using EAM potentials for the Pd and Cu interactions. The good agreement between the experimental data and the equilibrium simulation study leads us to conclude that the observed configurations of the film at different thicknesses correspond to the equilibrium state with thermally generated misfit dislocations as the strain relief mechanism. The microscopic nature of the misfit dislocation observed here for the Pd/Cu(100) system is rather complicated and does not fit into the simple model postulated previously [13].

On a microscopic level, the tensile-compressive asymmetry originates from the asymmetry of the interatomic interactions. The general feature of interatomic potentials is a steeply rising repulsive part at small separations as opposed to a very slowly decreasing attractive part at large

separations. This strong asymmetric feature of the interaction is what leads to the observed macroscopic tensile-compressive asymmetry. We have performed additional studies using very different potentials (of the Lennard-Jones-type) with the same general feature, and the results indeed remain qualitatively unchanged. Interestingly, we find that geometry and dimension play an important role in the tensile-compressive strain relief asymmetry. For the 2D model, misfit dislocations are favored for tensile rather than compressive strained systems [3,4]. Clearly, there is much more to learn in strain relief in heteroepitaxy through further theoretical and experimental investigations.

Y.L. acknowledges support from the MPI in Halle during his stay there. This work has been supported in part by Fundação de Amparo à Pesquisa do Estado de São Paulo - FAPESP (Grant No. 03/00541-0) (E. G.), the Academy of Finland through its Center of Excellence program (T. A.-N. and O. T.), and CRDF Grant No. RU-P1-2600-YA-04 (O.T.).

- 
- [1] J. W. Matthews, *J. Vac. Sci. Technol.* **12**, 126 (1975).
  - [2] Liang Dong, Jurgen Schnitker, Richard W. Smith, and David J. Srolovitz, *J. Appl. Phys.* **83**, 217 (1998).
  - [3] O. Trushin, E. Granato, S. C. Ying, P. Salo, and T. Ala-Nissila, *Phys. Rev. B* **65**, 241408 (2002).
  - [4] O. Trushin, E. Granato, S. C. Ying, P. Salo, and T. Ala-Nissila, *Phys. Rev. B* **68**, 155413 (2003).
  - [5] V. S. Stepanyuk, D. I. Bazhanov, W. Hergert, and J. Kirschner, *Phys. Rev. B* **63**, 153406 (2001); O. V. Lysenko, V. S. Stepanyuk, W. Hergert, and J. Kirschner, *Phys. Rev. Lett.* **89**, 126102 (2002); V. S. Stepanyuk, D. V. Tsviln, D. Sander, W. Hergert, and J. Kirschner, *Thin Solid Films* **428**, 1 (2003).
  - [6] H. Jenniches, J. Shen, Ch. V. Mohan, S. Sundar Manoharan, J. Barthel, P. Ohresser, M. Klaua, and J. Kirschner, *Phys. Rev. B* **59**, 1196 (1999).
  - [7] P. Ohresser, J. Shen, J. Barthel, M. Zheng, Ch. V. Mohan, M. Klaua, and J. Kirschner, *Phys. Rev. B* **59**, 3696 (1999).
  - [8] P. W. Murray, I. Stensgaard, E. Lægsgaard, and F. Besenbacher, *Phys. Rev. B* **52**, R14404 (1995); A. Bilic, Y. G. Shen, B. V. King, and D. J. O'Connor, *Surf. Rev. Lett.* **5**, 959 (1998); J. Kudrnovsky, S. K. Bose, and V. Drchal, *Phys. Rev. Lett.* **69**, 308 (1992).
  - [9] E. Hahn, E. Kampshoff, N. Wälchli, and K. Kern, *Phys. Rev. Lett.* **74**, 1803 (1995); I. A. Morrison, M. H. Kang, and E. J. Mele, *Phys. Rev. B* **39**, 1575 (1989); T. Kraft, P. M. Marcus, M. Methfessel, and M. Scheffer, *Phys. Rev. B* **48**, 5886 (1993).
  - [10] Y. S. Li, J. Quinn, H. Li, D. Tian, and F. Jona, *Phys. Rev. B* **44**, 8261 (1991).
  - [11] M. Zharnikov, A. Dittschar, W. Kuch, C. M. Schneider, and J. Kirschner, *Phys. Rev. Lett.* **76**, 4620 (1996).
  - [12] S. M. Foiles, M. I. Bakes, and M. S. Daw, *Phys. Rev. B* **33**, 7983 (1986).
  - [13] B. Müller, B. Fischer, L. Nedelmann, A. Fricke, and K. Kern, *Phys. Rev. Lett.* **76**, 2358 (1996).